Composites Science and Technology 87 (2013) 174–181

Contents lists available at ScienceDirect

Composites Science and Technology

journal homepage: www.elsevier.com/locate/compscitech

An in situ fabrication process for highly electrical conductive polyimide/MWCNT composite films using 2,6-diaminoanthraquinone

Yi-Chia Huang [a], June-Hua Lin [b], I-Hsiang Tseng [c], An-Ya Lo [d], Teng-Yuan Lo [a], Hsin-Pei Yu [e], Mei-Hui Tsai [e], Wha-Tzong Whang [a,*], Ken-Yuh Hsu [b]

[a] Department of Materials Science and Engineering, National Chiao Tung University, Hsinchu 30010, Taiwan, ROC
[b] Department of Photonics, National Chiao Tung University, Hsinchu 30050, Taiwan, ROC
[c] Department of Chemical Engineering, Feng Chia University, Taichung 40724, Taiwan, ROC
[d] Department of Materials Science and Engineering, Feng Chia University, Taichung 40724, Taiwan, ROC
[e] Department of Chemical and Materials Engineering, National Chin-Yi University of Technology, Taichung 41101, Taiwan, ROC

ARTICLE INFO

Article history:
Received 14 March 2013
Received in revised form 24 July 2013
Accepted 2 August 2013
Available online 16 August 2013

Keywords:
A. Carbon nanotubes
A. Nano composites
A. Polymer–matrix composites (PMCs)
Polyimide

ABSTRACT

We present a valuable in situ fabrication process for synthesizing high electrical conductive polyimide/multiwalled carbon nanotube (PI/MWCNT) composite films. The success of this process was achieved the addition of 2,6-diaminoanthraquinone (DAAQ). The DAAQ is not only an excellent dispersion agent to stably disperse pristine MWCNTs in solvent but also a monomer to directly synthesize PI. The strong interaction between DAAQ with MWCNT was verified by FTIR, UV–Vis, Raman, and fluorescence spectra. The highest value of electrical conductivity of 55.6 S/cm are achieved by the PI composite containing 40 wt.% of MWCNT. Moreover, the electrical conductivity of this film further enhanced to 106 S/cm after the thermal compression process. The MWCNT content at the percolation threshold of conductivity is 0.50 wt.% (or 0.32 vol.%) and the critical exponent is equal to 2.52. The developed in situ fabrication process through DAAQ-derived molecules can also be applied to synthesize other polymers requiring diamine structure.

1. Introduction

Polyimides (PIs) are widely used in the microelectronics industry such as flexible printed circuit boards, photoresists or dielectric interlayers in integrated circuits, aligning films in liquid crystal displays [1–3]. Many groups have made efforts in fabricating PI/CNT nanocomposites that with improved mechanical and electrical properties [4–9]. Carbon nanotubes (CNTs) exhibit excellent mechanical [4], electrical [5], thermal properties [10], and chemical stability [11–13], The strong van der Waals force among CNTs [14] leads to the aggregation of CNTs in composites or solutions and makes the homogeneous dispersion of CNTs in polymer matrix as a big challenge. To debundle and disperse the CNTs as individual tubes, many physical treatments and chemical modifications on CNTs have been published in literatures including acid modification [6,10,12–19], free-radical grafting [20–24], plasma treatment [25,26], and microwave irradiation [27–29]. Although the dispersion of CNT in polymer matrix may be greatly improved by those chemical treatments, the mechanical strength and electrical conductivity of the CNT are usually decreased significantly because of the shortened length of CNTs and the increased number of defects. In contrast, the physical method, by using surfactants has been widely applied to debundle and disperse CNT in polymer matrix [11,13,30–34] because the inherent property of CNTs can be maintained and the wetting ability of CNTs in composites will be increased. However, the remaining surfactants in the composites might degrade other properties of the composites. Yuan et al. [35] reported that CNTs disperse well in a specific poly(amic acid) (PAA) with hydroxyl groups on diamine monomer, and the resultant PI composite containing 30 wt.% of CNT shows a high electrical conductivity of 38.8 S/cm. Dispersion of CNTs is also affected by the types of solvent. N,N′-dimethylacetamide (DMAc) is a fair solvent to disperse and debundle CNTs because of the proper interaction between the alkyl amide groups and CNTs [36]. However, the CNT content is limited to low CNT concentration.

The aromatic diamine 2,6-diaminoanthraquinone (DAAQ) has been applied to produce self-assembly carbon nanofibers for field emission due to its strong intermolecular hydrogen bonding and π–π interactions [37,38]. The presence of π-orbitals or π-electrons on CNTs makes the π–π interactions between pristine CNTs and

* Corresponding author. Tel.: +886353731873.
E-mail address: wtwhang@mail.nctu.edu.tw (W.-T. Whang).

0266-3538/$ - see front matter © 2013 Published by Elsevier Ltd.
http://dx.doi.org/10.1016/j.compscitech.2013.08.008

DAAQ molecules possible. Hence, in this paper a time saving, energy saving, and cost saving (TEC) process is proposed to prepare polymer/CNT composite with the assistant of DAAQ. CNTs were first well dispersed in solvent DMAc with the presence of DAAQ, followed by the addition of dianhydride to perform in situ polymerization. The poly(amic acid)/CNT (PAA/CNT) solution will transform to PI/CNT composites after imidization. The resultant PI/CNT film containing 40 wt.% of CNT exhibits a high electrical conductivity of 106 S/cm after thermal compression process. To the best of our knowledge, this is the highest value among other literature reported ones. The stabilization of dispersed CNTs in polymer matrix is important because CNTs tend to re-agglomerate during the nanocomposites fabrication [39,40]. The DAAQ on MWCNTs can react with anhydride (one of starting materials for PI), preventing the dispersed MWCNTs from re-agglomeration due to the formation of protection layer on MWCNT surface. In our design the DAAQ molecule not only can well disperse CNT but also can be used in other synthetic reaction requiring diamines as the monomer or curing agent, such as the polymerization of polyurethanes, epoxy and polyamide. Hence, the TEC in situ fabrication process can widely be applied in preparing highly electrical conductive polymer/CNT composite films. The highly electrical conductive polymer/CNT composites have potential applications in photovoltaic devices [41], sensors [42], supercapacitors [43,44] and thermal diffusion materials.

2. Experimental

2.1. Materials

4,4′-(4,4′-isopropylidenediphenoxy)bis(phthalic anhydride) (IDPA, 97%, Aldrich) was purified by recrystallization using acetic anhydride (99.8%, Tedia). Molecular sieves (4 Å) were used to remove the water from the solvent. N,N′-dimethylacetamide (DMAc, HPLC, Tedia). 2,6-Diaminoanthraquinone (DAAQ, 97%) was purchased from Aldrich, pyromelliticdianhydride (PMDA) and oxydianiline (ODA) from Taimide Technology (Taiwan) and Multiwalled carbon nanotubes (MWCNTs, diameter: 40–90 nm and length: >10 μm) from Golden Innovation Co. (Taiwan) were stored in desiccators and used as received.

2.2. Fabrication of PI/MWCNT composite films

The preparation procedure of PI/MWCNT composites is shown in Fig. 1 MWCNTs were ultrasonication-assisted dispersed in DMAc for 30 min at a concentration of 3 mg/mL. Subsequently, stoichiometric amount of diamine DAAQ was added into the above solution under ultrasonication for another 15 min to obtain a homogeneous MWCNT–DAAQ suspension. Equalmolar dianhydride IDPA was divided into six fractions and each batch was sequentially stirred-mixed with the above mixture at room

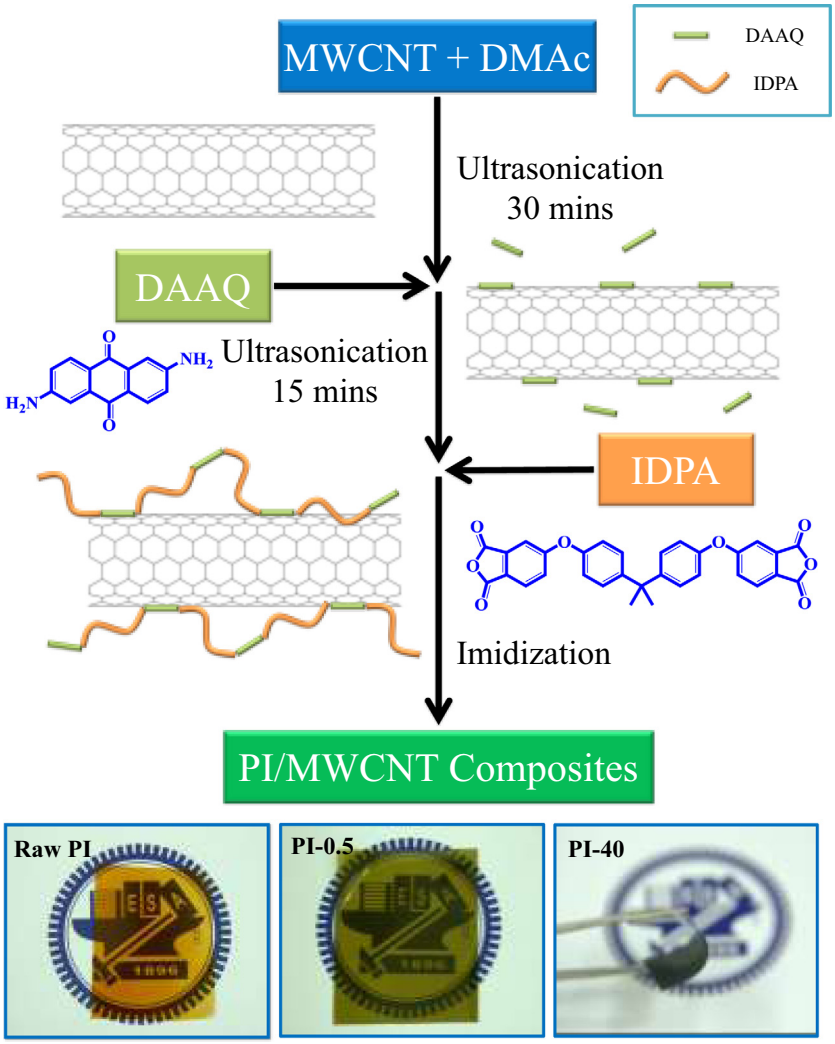

Fig. 1. Reaction scheme for synthesizing polyimide/MWCNT composite films.

temperature to obtain PAA/MWCNT solution. The above solution was then cast and step-wise thermal-imidized to 350 °C to acquire PI/MWCNT composite films. The sample is encoded PI–X, where X stands for the weight percentage of MWCNT in each sample. The photos of pure PI and PI/MWCNT composite films are shown in Fig. 1 PI-0.5 is transparent and PI-40 remains good flexibility. To investigate the effect of packing density on the electrical conductivity of the composite films, thermal compression was carried out on each film under the pressure of 3 kg/cm^2 at 350 °C for 1 h.

2.3. Characterization

UV–Vis absorption spectra were determined with a UV–Vis spectrometer (Shimadzu, UV1800). Fourier transform infrared (FTIR) spectra of PI, DAAQ and DAAQ-coated MWCNT were acquired by using a FTIR spectrophotometer (Nicolet, Protégé-460). Field emission scanning electron microscope (FE-SEM, JEOL, JSM-6700) and transmission electron microscope (TEM, JEOL, JEM-2010) were performed to observe the morphology of samples. Dynamic mechanical analyzer (DMA, TA Instruments, DMA 2980) was used to measure the storage modulus (E′) of samples under the frequency of 1 Hz and the heating rate of 3 °C/min from 60 °C to 300 °C. The electrical conductivities of PI/MWCNT composites were measured using a four-point probe electrical measurement device. A He—Ne laser with a wavelength of 632.8 nm was used as the light source in Raman spectroscope (Horiba Jobin–Yvon). Densities were measured in a density balance at 25 °C by weighting the samples in air (w_{air}) and then in water with the density of ρ_{water} (w_{water}). The density of the sample (ρ_{sample}) was calculated from the expression $\rho_{sample} = \rho_{water}\,(w_{air}/(w_{air}-w_{water}))$.

3. Results and discussions

3.1. Interaction between DAAQ and MWCNT

To compare the dispersion of MWCNTs within DMAC in the presence of ODA or DAAQ, MWCNTs mixed with ODA and DAAQ, respectively, were prepared. Fig. 2 exhibits the digital photographs of pristine MWCNT, MWCNT–ODA and MWCNT–DAAQ (DAAQ-coated MWCNT) in DMAc as a function of time. It is seen that dispersion of MWCNT–DAAQ hybrid is still homogeneous within one month, whereas the aggregation of MWCNT–ODA and pristine MWCNT occurred that coagulated bundles of tubes were presented at the bottom of their vials. The pristine MWCNT cannot maintain stably dispersed in DMAc but can be stably dispersed in DMAc with the presence of DAAQ for more than one month. The adsorption of DAAQ on the surface of MWCNT was revealed in the TEM micrograph (Fig. 2g) with the thickness of about 2 nm. In comparison, the surface of pristine MWCNT in Fig. 2f is clean without any adsorbate on it. The strong interaction of DAAQ with MWCNT can well disperse MWCNT in DMAc and increases the long-term stability of MWCNT suspension. The FTIR spectrum of pure PI is shown in Fig. 3a. The characteristic peaks of the PI were observed at 1782 cm^{-1} (C=O asymmetric stretch), 1720 cm^{-1} (C=O symmetric stretch), 1373 cm^{-1} (C—N stretch), and 740 cm^{-1} (C=O bending), indicating the successfully synthesis of PI from DAAQ and IDPA.

The FT-IR spectra of DAAQ, MWCNT and MWCNT–DAAQ were shown in Fig. 3b–d. The interactions between DAAQ and MWCNT were probed by measuring the shift in the DAAQ absorption peak before and after mixing with MWCNT. Two characteristic peaks near 1659 and 1627 cm^{-1} were associated with the non-symmetric and symmetric stretching vibration of C=O group in DAAQ. The non-symmetric C=O peak shifted from 1659 cm^{-1} for raw DAAQ to 1657 cm^{-1} for MWCNT–DAAQ. The absorption in the range of 3100–3650 cm^{-1} was resulted from —OH groups of MWCNT or —NH$_2$ of DAAQ. The broad peak of pristine MWCNT in 3200–3650 cm^{-1} is contributed by —OH groups. Both DAAQ and MWCNT–DAAQ displayed three N—H group peaks with various positions and intensities in the range of 3100–3650 cm^{-1} and the ratio or position of each peak changes. The peak near 3417 cm^{-1} is from the H-bonding-free N—H stretching, two peaks near 3325 and 3201 cm^{-1} are associated with the H-bonding of N—H stretching, one intramolecular H-bonding and the other intermolecular

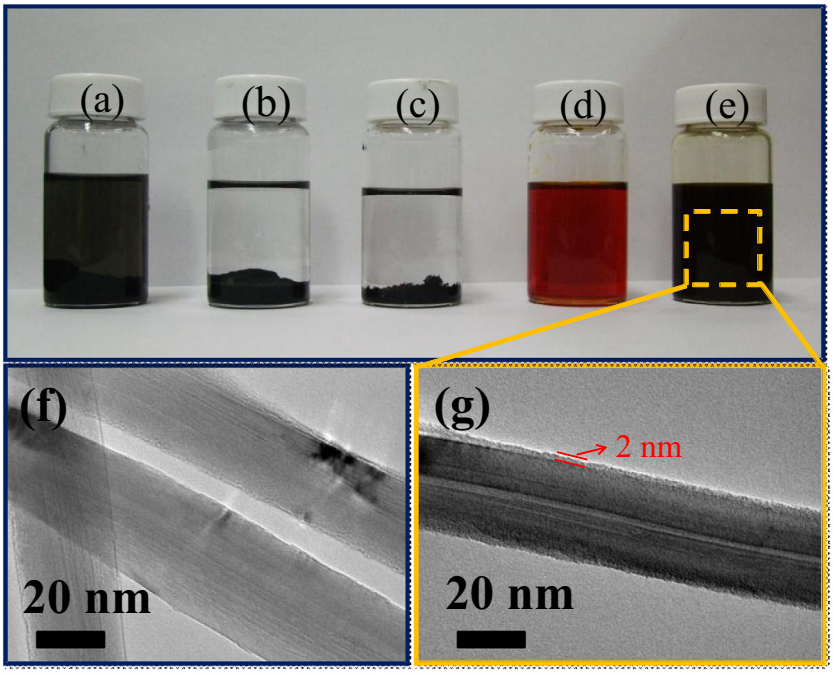

Fig. 2. Digital photographs of (a) MWCNT–ODA in DMAc for an hour, (b) MWCNT–ODA in DMAc for a month, (c) MWCNT in DMAc for a month (d) DAAQ in DMAc, and (e) MWCNT–DAAQ in DMAc for a month. TEM images of (f) MWCNT, (g) MWCNT–DAAQ.

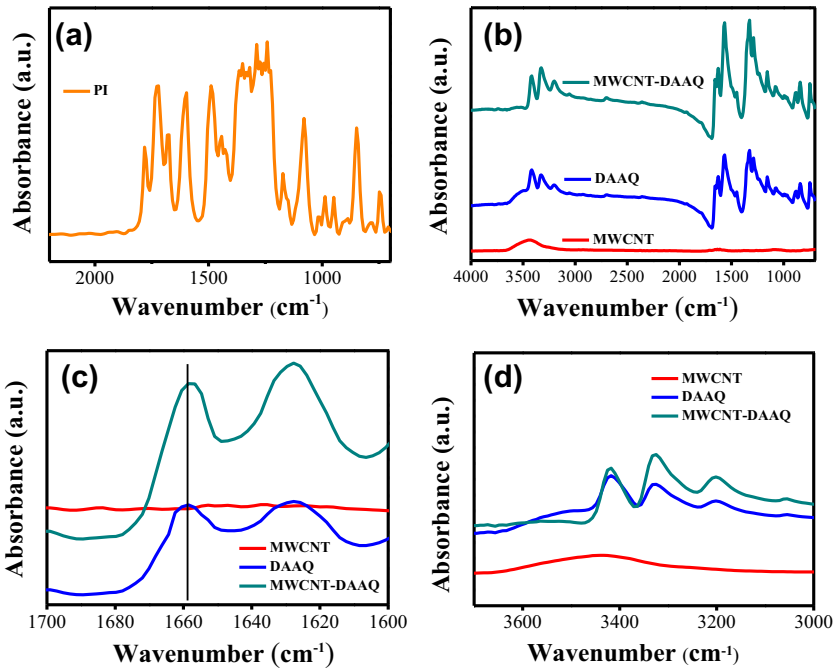

Fig. 3. The FTIR spectra of (a) PI, (b) DAAQ, MWCNT and MWCNT–DAAQ. The enlarged FTIR spectra of DAAQ, MWCNT and MWCNT–DAAQ in the range of (a) 1600–1700 cm^{-1} and (b) 3000–3700 cm^{-1}.

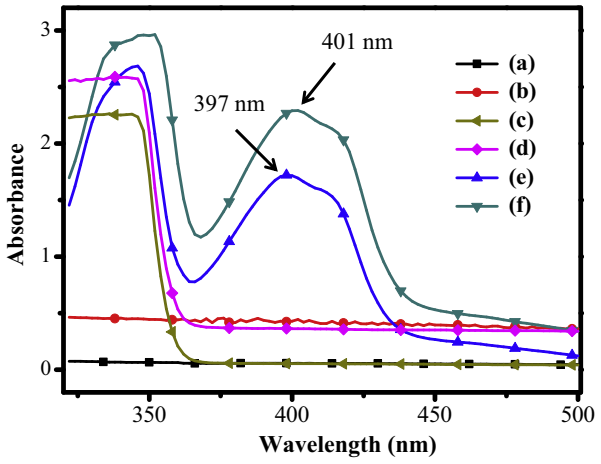

Fig. 4. The UV–Vis spectra of (a) DMAc, (b) MWCNT in DMAc, (c) ODA in DMAc, (d) MWCNT in DMAc with ODA, (e) DAAQ in DMAc and (f) MWCNT–DAAQ in DMAc.

H-bonding. Comparing with the peak intensity of H-bonding-free N—H stretching, MWCNT–DAAQ has more H-bonding N—H stretch than MWCNT suggesting the interactions between DAAQ and MWCNT.

The UV–Vis absorption spectra shown in Fig. 4 were utilized to further examine the interaction of DAAQ with MWCNTs. The absorption spectrum of pure DAAQ in DMAc solution has a peak assigned to the π–π^* transition around 397 nm. However, the π–π^* transition band shows a red shift from 397 to 401 nm for MWCNT–DAAQ in DMAc. The red shift is also found on other two peaks at 332 nm and 345 nm. The π–conjugation electrons of the dispersant can interact with those of carbon nanotube that the π–π interaction leads to a red shift [45]. This phenomenon was not occurred on MWCNT–ODA in DMAc.

Fluorescence spectroscopy was also applied to confirm the interaction between MWCNT and DAAQ. After being excited at a maximum adsorption wavelength of 345 nm, the DAAQ solution with the concentration of 1 μg/mL in DMAc exhibits the strong characteristic fluorescence at 558 nm as shown in the black curve in Fig. 5a. Similar spectral features are also displayed in the suspension of the MWCNT–DAAQ (1 μg/mL of MWCNT) as shown in the red curve in Fig. 5a. The fluorescence peak of MWCNT–DAAQ is much weaker than that of the peak of DAAQ. This phenomenon is interpreted as the π–π interaction between DAAQ and MWCNT that the strong fluorescence of DAAQ is efficiently quenched by MWCNT [46]. Moreover, the position of emission peak of DAAQ shifts by the presence of MWCNT. The emission peak shows a red shift from 558 nm for DAAQ in DMAc to 562 nm for the MWCNT–DAAQ in DMAc. This red shift phenomenon also supports the π–π interaction of DAAQ with MWCNT.

In addition, Fig. 5b shows the temporal profiles of emission recorded at 558 nm upon the excitation at 345 nm of two samples. The MWCNT–DAAQ shows faster emission decay and its fluorescence lifetime is shorten to 2.15 ns from 3.24 ns of DAAQ. It again suggests that the DAAQ emission is quenched by MWCNTs due to the strong interaction [30].

The Raman spectra of the MWCNT and MWCNT–DAAQ in Fig. 6 display two characteristic bands of MWCNTs at 1354 cm^{-1} (disorder mode) and 1572 cm^{-1} (tangential mode), which are called the D-band and G-band, respectively [47]. A G-band shift (from 1572 to 1577 cm^{-1}) is observed. This phenomenon is contributed from DAAQ, which modifies the electronic structure of CNTs [48,49]. The G-band at about 1572 cm^{-1} is related to the vibration of sp2-hybridized carbon atoms in a two-dimensional hexagonal lattice, such as in a graphitic layer. The D-band around 1354 cm^{-1} is associated with the presence of defects in the hexagonal graphitic layers [47]. The intensity ratio of the G-band to D-band (I_G/I_D) serves as a measure of the degree of graphitization of the MWCNTs; a higher degree of graphitization shows higher conductivity of MWCNT [50]. The values of I_G/I_D are about 10.2 and 10.4 of MWCNT and MWCNT–DAAQ, respectively. It shows that after MCWNTs were treated with DAAQ, the value of I_G/I_D maintains in the same level indicating the structure of MWCNT has not been

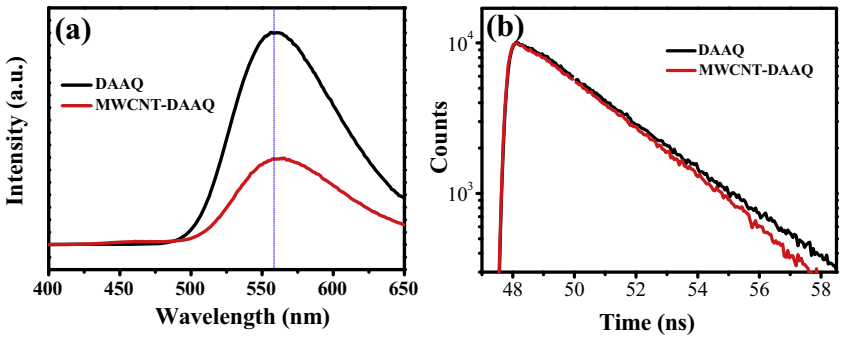

Fig. 5. (a) Fluorescence spectra (excited at 345 nm) and (b) decay curves of emission recorded at 558 nm.

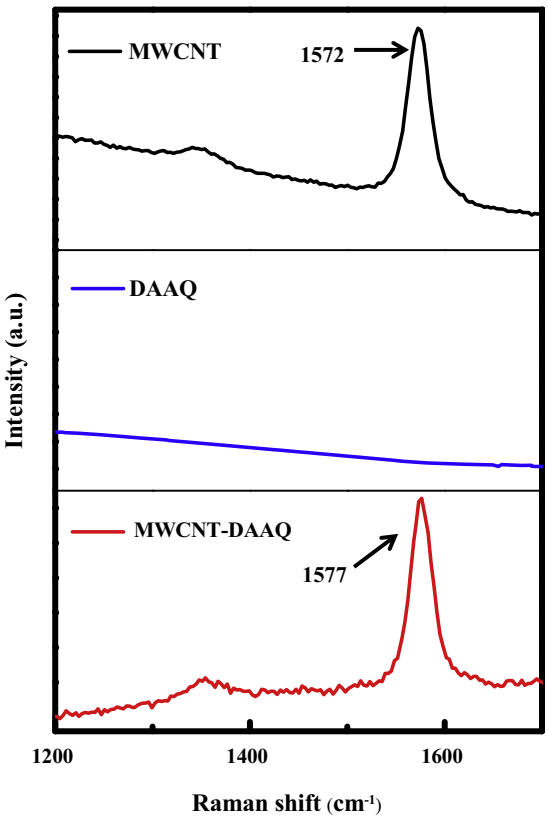

Fig. 6. The Raman spectra of MWCNT, DAAQ and MWCNT–DAAQ.

damaged. A little increase in the sp2-hybridization was due to the π–π interaction.

Fig. 7a and b shows the TEM images of MWCNT in reference PI derived from PMDA–ODA and PI-90 derived from DAAQ type. The surface of MWCNT in Fig. 7a is clean without any PI on it, in contrast, the surface of MWCNT in PI-90 is homogeneously covered with PI as shown in Fig. 7b. It means that DAAQ not only acts as a good dispersant of MWCNT in monomer solution but also have excellent interfacial interaction with MWCNT in the solid composite film. This result is consistent to Fig. 2g displaying 2 nm-thick layer of DAAQ adsorbed on the surface of MWCNT and explains why DAAQ disperses MWCNT very well in DMAc. Fig. 7 demonstrates SEM images of the cross-section of PI/MWCNT composite films including reference PI-0.5 (PMDA–ODA type) and DAAQ type PI-0.5. The MWCNT in Fig. 7c has clean surface and was detached from the PI matrix indicating the incompatibility to the PMDA–ODA type PI matrix. In contrast, the strong attachment of MWCNTs with PI matrix was revealed from the fracture surface of the DAAQ type PI-0.5. The PI derived from DAAQ is wetting well on the surface of MWCNT.

3.2. Characterization of PI/MWCNT composite films

Fig. 8a presents conductivity as a function of MWCNT content. The electrical conductivity of the DAAQ type PI/MWCNT composite films was promoted significantly by MWCNT. With the presence of 40 wt.% MWCNT in the composite film, the conductivity reaches up to 55.6 S/cm, compared to 5×10^{-16} S/cm for pure PI. Percolation theory predicts that the conductivity of composite film versus the volume fraction of carbon nanotube obeys the power law [51]: $\sigma \propto (V-V_c)^t$, where σ is the conductivity of the composite film, V the volume fraction of MWCNT, V_c the percolation threshold, and t the critical exponent. The fitting result was shown in the inset of Fig. 8a. The data of the composite films fitted to the above equation of Percolation theory gives the value of 0.32 vol.% (0.5 wt.%) for V_c and 2.52 for t.

Fig. 8b displays the linear dependence of the conductivities on MWCNT wt.% in as-prepared PI/MWCNT composites (black square) and the PI/MWCNT composites after thermal compression (red circle). The film conductivity increased to 106 S/cm for thermally compressed PI-40 compared to 10^{-16} S/cm for pure PI and 55.6 S/cm for as-prepared PI-40. The thermal compression process can easily enhanced the conductivity of films due to the increased film density as shown in Fig. 9.

The ideal densities were calculated from the wt.% in the composite films by the following equation: $1/\rho = (\omega/\rho_{MWCNT}) + [(1-\omega)/\rho_{PI}]$, where ω is weight percentage of MWCNT, ρ_{MWCNT} is the density of MWCNT and ρ_{PI} is the density of PI. The values of ρ_{MWCNT} and ρ_{PI} are 2.1 g/cm^3 and 1.21 g/cm^3, respectively. The film densities of the composite films, both as-prepared and thermally compressed films, deviate from the ideal densities as the MWCNT wt.% is higher than 10 wt.%. The higher the MWCNT wt.%, the greater the deviation, that is, there is more free volume in the films with more MWCNTs. the thermal compression increases the film density and reduces the deviation from the ideal density. Our previous study indicates that the conductivity is related to the amount of tube–tube junctions and the packing density [52]. The packing density and the number of tube–tube junctions are increased after thermal compression. Hence, the higher packing density and more tube–tube junctions of thermally compressed film endow higher electrical conductivity.

The storage moduli (E′) of the PI and PI/MWCNT composite films determined by DMA are shown in Fig. 10. The storage modulus of the composite films is enhanced distinctively with the increase of the MWCNT content at temperature $\leqq$200 °C. The storage modulus at 60 °C is increased from 1600 MPa for pure PI to 3200 MPa for PI-30 composite film. These demonstrate that the

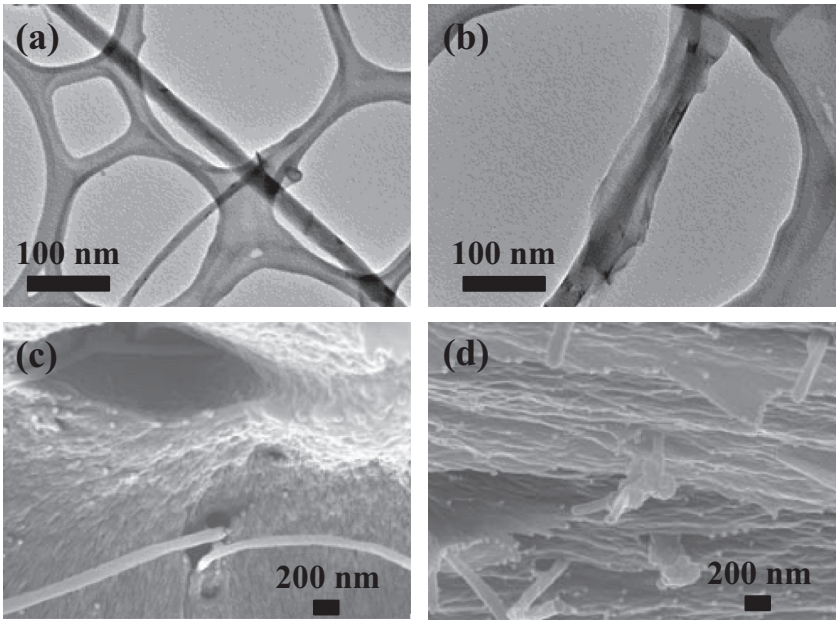

Fig. 7. Micrographs of TEM: (a) PMDA–ODA type PI containing 90 wt.% MWCNT and (b) PI-90 which containing 90 wt.% of MWCNT in PI derived from DAAQ. SEM images of the cross-section of PI/MWCNT composite films: (c) PMDA–ODA type PI-0.5 and (d) DAAQ type PI-0.5.

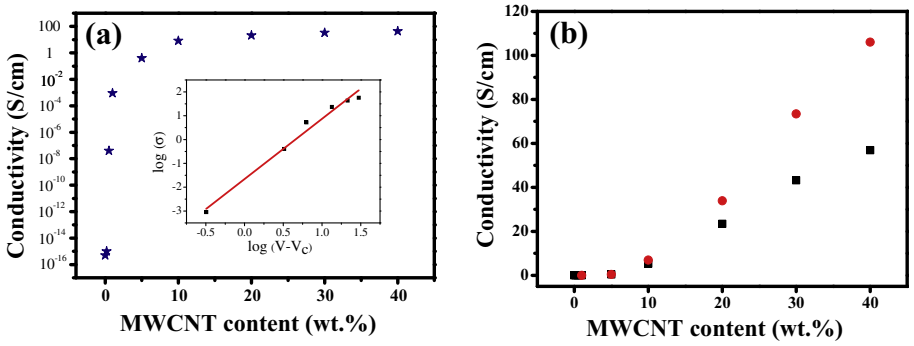

Fig. 8. (a) Conductivity as a function of MWCNT wt.% in DAAQ type PI/MWCNT composite films. The inset shows the fitting result by Percolation theory. (b) The conductivities versus MWCNT wt.% in as-prepared PI/MWCNT composite films (black square) and the PI/MWCNT composite films after thermal compression (red circle). (For interpretation of the references to color in this figure legend, the reader is referred to the web version of this article.)

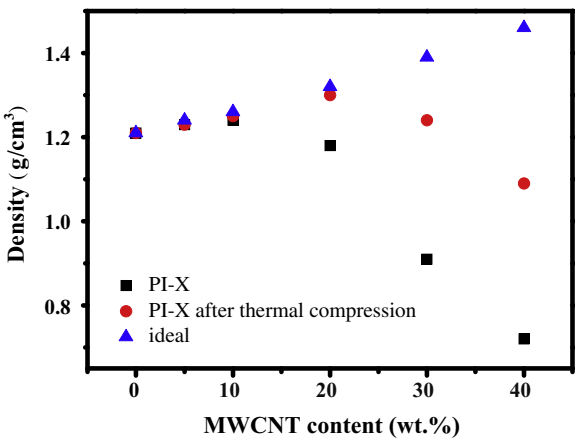

Fig. 9. The ideal densities and the real densities of DAAQ type PI/MWCNT composite films before and after thermal compression.

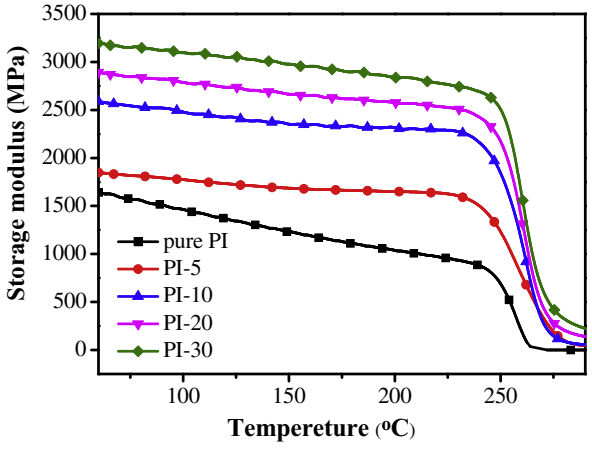

Fig. 10. The dynamic mechanical analysis for storage modulus of PI/MWCNT composite films with various MWCNT contents.

DAAQ-treated MWCNT promotes the mechanical modulus as well as the electrical conductivity of the composites.

4. Conclusions

In this paper, highly electrically conductive PI/MWCNT composite films were successfully synthesized by using DAAQ monomer. We have shown that DAAQ can well disperse MWCNT in DMAc and stablize the MWCNT in DMAc for as long time as one month. The strong π–π interaction of DAAQ with MWCNT has been verified by FTIR spectra, UV–Vis spectra, Raman spectra, and PL emission. DAAQ plays dual roles of a diamine monomer and an excellent MWCNT dispersant. The strong π–π interaction between DAAQ and MWCNT also endows excellent interfacial compatibility in the solid films as confirmed by TEM and SEM images. Well-dispersed MWCNT in PI matrix enhanced the conductivities that the highest conductivity of 55.6 S/cm has been achieved by as-prepared PI-40. The conductivity has been promoted to 106 S/cm after thermal compression the PI-40 film due to the enhanced packing density. Notably, these PI/MWCNT composite films display good flexibility. This innovative process through DAAQ-derived molecules can also be applied to synthesize other polymers requiring diamine structure.

Acknowledgements

The authors would like to acknowledge National Science Council of Taiwan (ROC) for the financial support through the projects NSC 99-2221-E-009-010-MY3 and 100-2221-E-009-023-MY3.

References

[1] Gosh MK, Mittal KL, editors. Polyimides: fundamentals and applications. New York: Marcel Dekker; 1996. p. 697–15.
[2] Chang CJ, Wu MS, Kao PC. Morphology and properties of low dielectric constant polymeric films with electrophoresis induced gradient close-pore distribution. Micropor Mesopor Mat 2008;111:267–75.
[3] Chang CJ, Chou RL, Lin YC, Liang BJ, Chen JJ. Effects of backbone conformation and surface texture of polyimide alignment film on the pretilt angle of liquid crystals. Thin Solid Films 2011;519:5013–6.
[4] Iijima S. Helical microtubules of graphitic carbon. Nature 1991;354:56–8.
[5] Jiang X, Bin Y, Matsuo M. Electrical and mechanical properties of polyimide-carbon nanotubes composites fabricated by in situ polymerization. Polymer 2005;46:7418–24.
[6] So HH, Cho JW, Sahoo NG. Effect of carbon nanotubes on mechanical and electrical properties of polyimide/carbon nanotubes nanocomposites. Euro Polym J 2007;43:3750–6.
[7] Chou WJ, Wang CC, Chen CY. Polym Degrad Stabil 2008;93:745–52.
[8] Choi BG, Park H, Park TJ, Kim DH, Lee SY, Hong WH. Development of the electrochemical biosensor for organophosphate chemicals using CNT/ionic liquid bucky gel electrode. Electrochem Commun 2009;11:672–5.
[9] Subramoney S. Novel nanocarbons—structure, properties, and potential applications. Adv Mater 1998;10:1157–71.
[10] Yuen SM, Ma CCM, Lin YY, Kuan HC. Preparation, morphology and properties of acid and amine modified multiwalled carbon nanotube/polyimide composite. Compos Sci Technol 2007;67:2564–73.
[11] Tang QY, Chan YC, Wong NB, Cheung R. Surfactant-assisted processing of polyimide/multiwall carbon nanotube nanocomposites for microelectronics applications. Polym Int 2010;59:1240–5.
[12] Zhu BK, Xie SH, Xu ZK, Xu YY. Preparation and properties of the polyimide/multi-walled carbon nanotubes (MWNTs) nanocomposites. Compos Sci Technol 2006;66:548–54.
[13] Tang QY, Chen J, Chan YC, Chung CY. Effect of carbon nanotubes and their dispersion on thermal curing of polyimide precursors. Polym Degrad Stabil 2010;95:1672–8.
[14] Jiang LY, Huang Y, Jiang H, Ravichandran G, Gao H, Hwang KC, et al. A cohesive law for carbon nanotube/polymer interfaces based on the van der Waals force. J Mech Phys Solids 2006;54:2436–52.
[15] Ma Y, Zheng Y, Wei G, Song W, Hu T, Yang H, et al. Processing, structure, and properties of multiwalled carbon nanotube/poly(hydroxybutyrate-co-valerate) biopolymer nanocomposites. J Appl Polym Sci 2012;125:E620–9.
[16] Wang J, Wei N, Wang F, Wu C, Li S. High-dielectric constant percolative composite of P(VDF-TrFE) and modified multi-walled carbon-nanotubes. Polym Bull 2012;68:2285–97.
[17] Kuan HC, Ma CCM, Chang WP, Yuen SM, Wu HH, Lee TM. Synthesis, thermal, mechanical and rheological properties of multiwall carbon nanotube/waterborne polyurethane nanocomposite. Compos Sci Technol 2005;65:1703–10.
[18] Kuznetsova A, Mawhinney DB, Naumenko V, Yates JT, Liu J, Smalley RE. Enhancement of adsorption inside of single-walled nanotubes: opening the entry ports. Chem Phys Lett 2000;321:292–6.
[19] Liu P. Modifications of carbon nanotubes with polymers. Euro Polym J 2005;41:2693–703.
[20] Yuen SM, Ma CCM, Chiang CL, Teng CC, Yu YH. Poly(vinyltriethoxysilane) modified MWCNT/polyimide nanocomposites—preparation, morphological, mechanical, and electrical properties. J Polym Sci Pol Chem 2008;46:803–16.
[21] Teng CC, Ma CCM, Chiou KC, Lee TM, Shih YF. Synergetic effect of hybrid boron nitride and multi-walled carbon nanotubes on the thermal conductivity of epoxy composites. Mater Chem Phys 2011;126:722–8.
[22] Lou X, Detrembleur C, Sciannamea V, Pagnoulle C, Jerome R. Grafting of alkoxyamine end-capped (co)polymers onto multi-walled carbon nanotubes. Polymer 2004;45:6097–102.
[23] Liu Y, Yao Z, Adronov A. Functionalization of single-walled carbon nanotubes with well-defined polymers by radical coupling. Macromolecules 2005;38:1172–9.
[24] Chang CM, Liu YL. Functionalization of multi-walled carbon nanotubes with non-reactive polymers through an ozone-mediated process for the preparation of a wide range of high performance polymer/carbon nanotube composites. Carbon 2010;48:1289–97.
[25] Chou WJ, Wang CC, Chen CY. Characteristics of polyimide-based nanocomposites containing plasma-modified multi-walled carbon nanotubes. Compos Sci Technol 2008;68:2208–13.
[26] Tseng CH, Wang CC, Chen CY. Functionalizing carbon nanotubes by plasma modification for the preparation of covalent-integrated epoxy composites. Chem Mater 2007;19:308–15.
[27] Shim HC, Kwak YK, Han CS, Kim S. Enhancement of adhesion between carbon nanotubes and polymer substrates using microwave irradiation. Scripta Mater 2009;61:32–5.
[28] Wang CY, Chen TH, Chang SC, Cheng SY, Chin TS. Strong carbon-nanotube–polymer bonding by microwave irradiation. Adv Funct Mater 2007;17:1979–83.
[29] Lin W, Moon KS, Wong CP. A combined process of in situ functionalization and microwave treatment to achieve ultrasmall thermal expansion of aligned carbon nanotube–polymer nanocomposites: toward applications as thermal interface materials. Adv Mater 2009;21:2421–4.
[30] Yan YH, Cui J, Zhao S, Zhang JF, Liu JW, Cheng JM. Interface molecular engineering of single-walled carbon nanotube/epoxy composites. J Mater Chem 2012;22:1928–36.
[31] Tasis D, Tagmatarchis N, Bianco A, Prato M. Chemistry of carbon nanotubes. Chem Rev 2006;106:1105–36.
[32] Liu X, Chan-Park MB. Facile way to disperse single-walled carbon nanotubes using a noncovalent method and their reinforcing effect in poly(methyl methacrylate) composites. J Appl Polym Sci 2009;114:3414–9.
[33] Zorbas V, Ortiz-Acevedo A, Dalton AB, Yoshida MM, Dieckmann GR, Draper RK, Baughman RH, Jose-Yacaman M, Musselman IH. Preparation and characterization of individual peptide-wrapped single-walled carbon nanotubes. J Am Chem Soc 2004;126:7222–7.
[34] Zhu J, Kim JD, Peng H, Margrave JL, Khabashesku VN, Barrera EV. Improving the dispersion and integration of single-walled carbon nanotubes in epoxy composites through functionalization. Nano Lett 2003;3:1107–13.
[35] Yuan W, Che J, Chan-Park MB. A novel polyimide dispersing matrix for highly electrically conductive solution-cast carbon nanotube-based composite. Chem Mater 2011;23:4149–57.
[36] Landi BJ, Ruf HJ, Worman JJ, Raffaelle RP. Effects of alkyl amide solvents on the dispersion of single-wall carbon nanotubes. J Phys Chem B 2004;108:17089–95.
[37] Sasirekha V, Ramakrishnan V. Study of preferential solvation of 2,6-diaminoanthraquinone in binary mixtures by absorption and fluorescence studies. Spectrochim Acta A 2008;70:626–33.
[38] Huang KJ, Hsiao YS, Whang WT. Low-temperature formation of self-assembled 1,5-diaminoanthraquinone nanofibers: substrate effects and field emission characteristics. Org Electron 2011;12:686–93.
[39] Bryning MB, Islam MF, Kikkawa JM, Yodh AG. Very low conductivity threshold in bulk isotropic single-walled carbon nanotube–epoxy composites. Adv Mater 2005;17:1186–91.
[40] Ma PC, Mo SY, Tang BZ, Kim JK. Dispersion, interfacial interaction and re-agglomeration of functionalized carbon nanotubes in epoxy composites. Carbon 2010;48:1824–34.
[41] Kymakis E, Amaratunga GAJ. Single-wall carbon nanotube/conjugated polymer photovoltaic devices. Appl Phys Lett 2002;80:112–4.
[42] Chen HW, Wu RJ, Chan KH, Sun YL, Su PG. The application of CNT/Nafion composite material to low humidity sensing measurement. Sens Actuat B – Chem 2005;104:80–4.
[43] Frackowiak E, Khomenko V, Jurewicz K, Lota K, Béguin F. Supercapacitors based on conducting polymers/nanotubes composites. J Power Source 2006;153:413–8.
[44] Zhou CF, Kumar S, Doyle CD, Tour JM. Functionalized single wall carbon nanotubes treated with pyrrole for electrochemical supercapacitor membranes. Chem Mater 2005;17:1997–2002.
[45] Zhang H, Li HX, Cheng HM. Water-soluble multiwalled carbon nanotubes functionalized with sulfonated polyaniline. J Phys Chem B 2006;110:9095–9.

[46] Chen J, Liu H, Weimer WA, Halls MD, Waldeck DH, Walker GC. Noncovalent engineering of carbon nanotube surfaces by rigid, functional conjugated polymers. J Am Chem Soc 2002;124:9034–5.
[47] Madni I, Hwang CY, Park SD, Choa YH, Kim HT. Mixed surfactant system for stable suspension of multiwalled carbon nanotubes. Colloid Surf A 2010; 358:101–7.
[48] Klinke C, Chen C, Afzali A, Avouris P. Charge transfer induced polarity switching in carbon nanotube transistors. Nano Lett 2005;5:555–8.
[49] Ma PC, Zheng QB, Mäder E, Kim JK. Behavior of load transfer in functionalized carbon nanotube/epoxy nanocomposites. Polymer 2012;53:6081–8.
[50] Vaisman L, Wagner HD, Marom G. The role of surfactants in dispersion of carbon nanotubes. Adv Colloid Interface 2006;128–130:37–46.
[51] Sandler JKW, Kirk JE, Kinloch IA, Shaffer MSP, Windle AH. Ultra-low electrical percolation threshold in carbon-nanotube-epoxy composites. Polymer 2003;44:5893–9.
[52] Ryu Y, Yin L, Yu C. Dramatic electrical conductivity improvement of carbon nanotube networks by simultaneous de-bundling and hole-doping with chlorosulfonic acid. J. Mater Chem 2012;22:6959–64.